


Supercurrent rectification effect in graphene-based Josephson junctions

Ya-Jun Wei,^{*} Han-Lin Liu^{✉,*} and J. Wang^{✉†}
School of Physics, Southeast University, Nanjing 210096, China

Jun-Feng Liu[‡]
School of Physics and Materials Science, Guangzhou University, Guangzhou 510006, China

 (Received 17 May 2022; revised 15 August 2022; accepted 5 October 2022; published 19 October 2022)

We report a theoretic study of the supercurrent rectification effect in the graphene-based superconductor (GS) junction without invoking any spin-related interaction. By introducing the valley coupling effect through the Kekulé lattice distortion as well as the valley polarization interaction, we demonstrate that the GS/G/GS Josephson junction (JJ) can exhibit not only a π -state JJ but also a ϕ_0 -state one, in which a nonzero supercurrent can flow without the superconducting phase difference between the two GS electrodes. A supercurrent rectification effect, that the critical supercurrent is asymmetric between the two opposite flowing directions, is identified. The conditions for the optimal supercurrent rectification effect are also discussed.

DOI: [10.1103/PhysRevB.106.165419](https://doi.org/10.1103/PhysRevB.106.165419)

I. INTRODUCTION

Josephson junction (JJ) has been one of the most extensive and intensive research subjects for decades, because it has the fundamental research interest as well as realistic applications in making superconducting electronic devices like SQUID [1–7]. For example, a π -state JJ has been proposed as a circuit element for quantum computation and as on-chip π phase shifters for various self-biasing quantum/classical circuits [8–10]. Recently, the supercurrent rectification effect (SRE) has been observed experimentally in the superconductor films [11–13] and JJ systems [14–18], and has already ignited a surge of interest in the research community to study such nonreciprocal phenomenon in the superconductor systems [19–23].

The SRE or superconductor diode effect is referred to as the phenomenon that the forward critical supercurrent is unequal to the backward (reversal) one in superconductor systems, and as a result, a charge current with the magnitude in between them might be in a nonresistive state flowing in one direction but dissipative in the opposite direction. This is in a striking contrast with the conventional resistive semiconductor diode. Two gradients, the broken time-reversal symmetry and broken space-inversion symmetry, are vital for the SRE. The former one would give rise to a nonzero momentum for Cooper pairs while the latter generally produces a strong spin-orbit interaction so that the excitation energy of quasiparticles would depend on the momentum direction linearly, thus the critical supercurrent could be asymmetric over a certain momentum direction [19]. At present, all observed or proposed

SRE were shown in the systems with a strong spin-orbit interaction plus an external magnetic field or magnetization breaking the two mentioned symmetries [24]. Without spin-related interactions, such an SRE from other factors like the valley-related interactions has not been studied so far.

The graphene-based JJ was experimentally fabricated by depositing two closely spaced superconductor electrodes on graphene (G) [25–29], where the proximity effect is responsible for the superconductivity generated in graphene. As is known, there is an extra valley degree of freedom of Dirac electrons termed as K and K' , which are related to each other via the time-reversal symmetry like the spin degree of freedom. The valley polarization of electrons in graphene was proposed by employing an external electromagnetic radiation in the terahertz frequency range [30,31]. In addition, the valley polarization was also verified in the magic-angle twisted bilayer graphene system, which is attributed to the electron-electron interaction [32]. Based on this valley polarization, a ϕ_0 -state JJ has been recently proposed in the twisted bilayer graphene system [33].

In the monolayer graphene system, the graphene superlattice with a certain Kekulé lattice distortion could be found when graphene was grown upon a specific substrate. Such Kekulé structure would usually lead to a valley coupling effect. For example, a recent experiment [34] demonstrated that a graphene superlattice with Y-shaped Kekulé distortion can grow epitaxially onto Cu(111), with the copper atoms in registry with the carbon atoms and one of six carbon atoms in each superlattice unit cell (larger than the original graphene unit cell) has no copper atom below it, so a Cu vacancy in substrate is forming. The valley coupling effect has been extensively investigated to control and modulate the valley-related transport of Dirac electrons [35–40].

In this work, we study the possible ϕ_0 -state JJ and the SRE in the graphene superconductor (GS) junction by invoking the valley-related interactions instead of the usual spin

^{*}This authors contributed equally to this work and should be considered co-first authors.

[†]jwang@seu.edu.cn

[‡]phjliu@gzhu.edu.cn

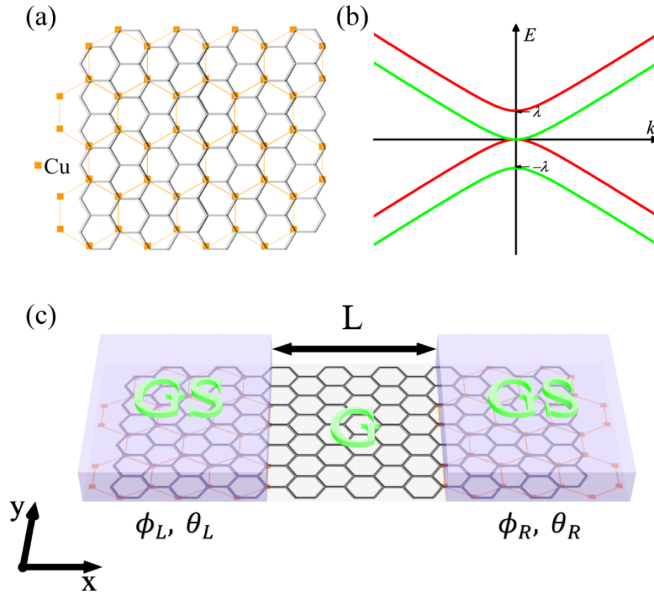


FIG. 1. (a) A schematic Kekulé graphene superlattice grown on a Cu substrate. One Cu vacancy on each C-atom hexagon consists in a commensurate enlarged superlattice structure with the unit cell of $\sqrt{3}a \times \sqrt{3}a$, where a is the graphene lattice constant. (b) Electronic band structure of the simplified model for the Kekulé structure. The two Dirac bands are split due to the valley coupling effect with the splitting energy $\pm\lambda$. (c) Setup of the GS/G/GS JJ. The GS is formed by putting an s -wave superconductor onto the Kekulé structure while the left and right GSs have different lattice axis directions represented by $\theta_{L(R)}$. $\phi_{L(R)}$ denotes the left (right) superconducting phase. In the middle G region ($0 < x < L$) the valley polarization interaction is introduced.

interactions. When the two GS electrodes have different Kekulé structures, the introduced valley polarization could lead to both π -state JJ and ϕ_0 -state junction, and moreover, the SRE in the ϕ_0 -state JJ can be controlled by the valley interactions. When the universal chemical potential locates just above the bottom of the upper split energy band due to the Kekulé distortion [see Fig. 1(b)], an optimal SRE would arise.

This work is organized as follows. In Sec. II, we introduce the GS/G/GS junction model and describe the valley coupling and polarization interactions. In Sec. III, numerical calculations of the supercurrent flowing in the JJ are present. The condition for obtaining an optimal SRE is discussed in Sec. IV. A brief conclusion is drawn in the last section.

II. MODEL

The valley coupling effect in graphene can be generally realized through the graphene superlattice structure from either the lattice commensurate substrate [41] or periodic adatoms [42], thus the unit cell is enlarged by $\sqrt{3} \times \sqrt{3}$ and the original K and K' valleys of the pristine graphene are folded into the Γ point. We consider the Y-type Kekulé structure demonstrated in experiment [34] through the periodic Cu substrate to grow graphene and the superlattice is schematically shown in Fig. 1(a), where one C atom of each hexagon sits on a Cu vacancy. Note that the other type of lattice distortion leading

to the valley coupling effect can exert the same effect as the Y-type Kekulé structure, since the main role from the lattice distortion is the valley coupling. The Y-type Kekulé structure we adopted here is the same as the periodic adatoms-modified graphene studied in Ref. [42], which is described as

$$H_k = \hbar v_f (\tau_z \sigma_x k_x + \sigma_y k_y) + \frac{\lambda}{2} (1 + \sigma_z) (\tau_x \cos \theta + \tau_y \sin \theta), \quad (1)$$

where $\sigma_{x,y,z}$ is the lattice pseudospin operator, $\tau_{x,y,z}$ is the valley Pauli operator, and $k_{x,y}$ is the 2D momentum. The second term denotes the valley coupling effect with the strength λ . θ represents the lattice axis direction of the graphene superlattice and is meaningless in a homogeneous system. The valley coupling fulfills the time-reversal symmetry and the Kekulé lattice keeps a rotational symmetry, so it is essentially different from the spin-orbit interaction which stems from the potential asymmetry or lack of inversion symmetry center. It is noted that the above Hamiltonian stems from the original site energy modifications to the graphene due to the periodic Cu vacancy in the substrate and the hopping energy modifications are neglected. The eigenvalues of the above Hamiltonian are simply given by ($\hbar v_f = 1$),

$$E = \pm \lambda/2 \pm \sqrt{\lambda^2/4 + k^2}, \quad (2)$$

with $k^2 = k_x^2 + k_y^2$. The corresponding band structure is plotted in Fig. 1(b), where the two (valley-helical) bands are split with the band gap magnitude λ ; this case is also termed as the single valley Dirac band [42]. In fact, the valley coupling strength λ originates from the site energy modification to the graphene lattice, while the hopping energy modification leading to the valley-orbit coupling effect due to the Kekulé distortion is neglected here for simplicity, and moreover, it would not make a qualitative difference.

It is assumed that the GS is obtained through the superconducting proximity effect [25,26] and the GS/G/GS model is schematically shown in Fig. 1(c). The left and right GSs have a different superconducting phase $\phi_L = -\phi_R = \phi/2$. $\theta_L = -\theta_R = \theta/2$ is the different azimuthal angle of the left and right lattice axis directions. The length of the normal G region is L and the introduced valley polarization effect is limited in this region. The valley polarization can be realized experimentally by using external optical irradiations [30,31] but theoretically, it can also be implemented by using magnetization plus the intrinsic spin-orbit interaction in graphene [43,44]. The latter scheme is not taken into account here because the spin-related interactions are not invoked in this work. A simplified valley polarization term like the spin exchange interaction [45] is described by

$$H_{vp} = \tau_z h_z, \quad (3)$$

where h_z simulates simply the *valley exchange field* with an energy unit. It is noted that the field h_z should break the time reversal symmetry unlike the λ term.

The GS Hamiltonian is given by

$$H_{sc} = \begin{pmatrix} H_k + H_{vp} - \mu & \Delta e^{i\phi} \\ \Delta e^{-i\phi} & \mu - \mathcal{T}(H_k + H_{vp})\mathcal{T}^{-1} \end{pmatrix}, \quad (4)$$

with \mathcal{T} being the time-reversal symmetry operator,

$$\mathcal{T} = \begin{pmatrix} 0 & I \\ I & 0 \end{pmatrix} \mathcal{K}, \quad (5)$$

where I is a unit matrix, \mathcal{K} is the complex conjugate operator, and Δ is the pair potential strength with the superconducting phase ϕ . For the GS/G/GS junction, the left and right electrode Hamiltonians H_{sc} are different in $\phi_{L,R}$ as well as $\theta_{L,R}$. The valley polarization is limited in the normal G region ($0 < x < L$) as stated above.

We employ a numerical method to calculate the Josephson current by discretizing the real space and mapping the above Hamiltonian onto a quasi-one-dimensional (Q1D) tight-binding-like model, e.g., H_k is transformed as

$$H_k = \sum_{j\alpha\beta k_y} \left\{ \left[-i\frac{t}{2} C_{j+1,\alpha k_y}^+ \tau_z \sigma_x C_{j\beta k_y} - t_p C_{j+1,\alpha k_y}^+ \sigma_z C_{j\beta k_y} + \text{H.c.} \right] \right. \\ \left. + t \sin(k_y a) C_{j\alpha k_y}^+ \sigma_y C_{j\beta k_y} + \frac{\lambda}{2} (\cos \theta \tau_x + \sin \theta \tau_y) C_{j\alpha k_y}^+ \right. \\ \left. \times (\sigma_0 + \sigma_z) C_{j\beta k_y} + (4t_p - 2t_p \cos k_y a) C_{j\alpha k_y}^+ \sigma_z C_{j\beta k_y} \right\}, \quad (6)$$

where $C_{j\alpha(\beta)k_y}^+$ ($C_{j\alpha(\beta)k_y}$) is the electron creation (annihilation) operator, j is the 1D lattice site index, $\alpha(\beta)$ is the pseudospin lattice operator, k_y is the transverse momentum, and $t = \hbar v_f/a$ is the hopping term of electrons with a being the lattice constant. t_p is introduced to avoid the valley degeneracy at the Brillouin edge ($k_x, k_y = \pm\pi/a$) since only one valley at the Brillouin center ($\mathbf{k} = 0$) is studied. H_{vp} and H_{sc} can be transformed in the same way. Notice that the discretization is just along the x axis and while the k_y momentum remains in a continuum form, i.e., the above Hamiltonian is in a mixed Bloch and lattice representation. Equation (1) can be fully recovered from the above Hamiltonian by transforming the x -directed lattice with approximation of $k_x a \sim 0$, $k_y a \sim 0$ to the continuum limit.

Since the charge current is conserved in the nonsuperconductor region, it can be evaluated in the normal G region of the JJ at any site j as

$$I = \frac{e}{h} \int dE \sum_{k_y} \text{Tr} \{ [t_{j,j+1} G_{j+1,j}^< - \text{H.c.}] s_z \}, \quad (7)$$

where $G_{j,j+1}^<$ is the lesser Green's function and $G^< = (G^a - G^r) f(E)$ in equilibrium, $t_{j,j+1}$ is hopping matrix between two neighboring sites of the Q1D lattice model, s_z denotes the z component of the Pauli operator of the $e-h$ space, the trace is over the valley τ , pseudolattice spin σ , and superconducting $e-h$ spaces s . $f(E)$ is the Fermi-Dirac distribution function. $G^r = (EI - H_c - \Sigma_L - \Sigma_R)^{-1}$ is the retarded Green's function ($G^a = [G^r]^\dagger$), where I is a unit matrix and H_c is the Hamiltonian describing the normal G region of the studied JJ in the Nambu space, while $\Sigma_{L(R)}$ is the self-energy of the left (right) GS and can be calculated with a usual recursive method [46].

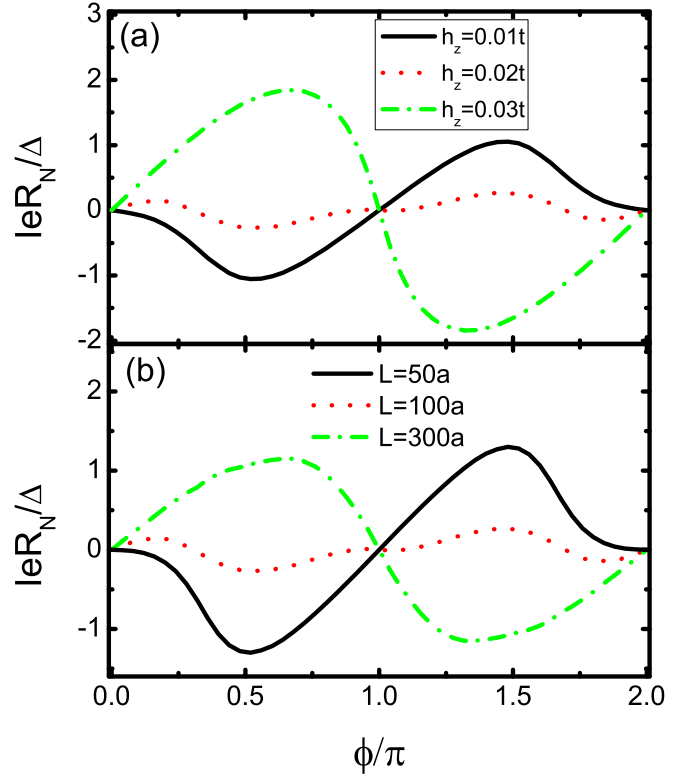


FIG. 2. Supercurrent phase relation $I(\phi)$ with different valley polarization h_z (a) and different the JJ length L (a). Parameters are $\mu = 0.05t$, $\lambda = 0.03t$, $\theta = 0$, and $L = 100a$ in (a), and $h_z = 0.02t$ in (b).

III. RESULTS

In numerics, the hopping energy is set as the energy unit $t = 1$ eV, the universal chemical potential is taken as $\mu = 0.05t$, and the zero-temperature is considered in this work. No external bias or static potential is taken into account. The superconducting coherence length is estimated to be $\xi_s = \hbar v_f/\Delta = 1000a$ with the pair potential set as $\Delta = 0.001t$. The $t_p = 0.3t$ is set in Eq. (6) for removing the valley degeneracy when the Q1D lattice model is mapped from the continuum one.

We first set the azimuthal angle zero, $\theta = \theta_L - \theta_R = 0$, which means the GS/G/GS junction has the left-right parity symmetry and $I(\phi) = -I(-\phi)$. In Fig. 2, the current-phase relation $I(\phi)$ is plotted with different valley polarization strengths h_z and the junction lengths L . R_N in the current unit denotes the junction resistance of the normal junction without superconducting pair potentials. It is shown that the supercurrent direction for a fixed ϕ would be reversed with a variation of h_z in Fig. 2(a) or L in Fig. 2(b), i.e., these two parameters can be used to modulate the so-called $0-\pi$ state transition. The physics is that the valley polarization term h_z can give rise to an extra phase shift to the Cooper pairs traveling in the normal G region, and as a result, the JJ's ground state can be stabilized either at $\phi = \pi$ or at $\phi = 0$.

Although the valley coupling effect is considered in the above current-phase relations, there is no ϕ_0 -state JJ found [$I(\phi = 0) = 0$]. Unlike the spin-orbit interaction, the Kekulé

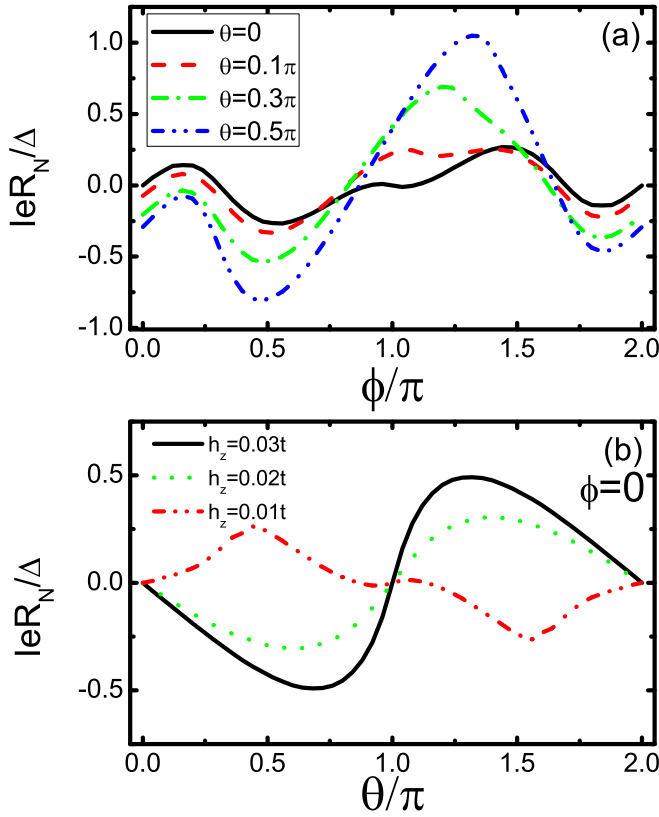


FIG. 3. Supercurrent phase relation $I(\phi)$ with different azimuthal angles θ (a) and the zero phase ($\phi = 0$) supercurrent as a function of the azimuthal angle θ . Parameters are $\mu = 0.05t$, $\lambda = 0.03t$, $L = 100a$, and $h_z = 0.02t$ in (a).

graphene structure does not result from the broken inversion symmetry and moreover, the system still holds the parity (inversion) symmetry along x or y direction in the discrete lattice model. Hence, we can instead choose a nonuniform Kekulé structure via nonzero θ to simulate the broken space inversion symmetry. Under this circumstance, the valley coupling term may not be limited in the two GS electrodes and can indeed extend to the normal G region, however, its inhomogeneity in real space is still necessary for possible ϕ_0 -state JJ as shown in Fig. 3.

When $\theta \neq 0$, there exists a nonzero supercurrent at zero phase difference $\phi = 0$, $I(\phi = 0) \neq 0$, as shown in Fig. 3(a). The zero supercurrent at $\phi = \phi_0$ becomes even more evident with an increase of θ . In Fig. 3(b), $I(\phi = 0)$ is plotted as a function of θ and it is almost a sine function of θ . Nevertheless, the current magnitude and direction can be modulated by h_z . It is also shown that the magnitude of $I(\phi = 0)$ is quite small in comparison with the forward (backward) critical current I_c^\pm . This indicates that θ should not directly enter the superconducting phase ϕ , in other words, the ϕ_0 phase shift may not stem from the bulk effect of the valley coupling, but from the interface scattering effect.

In Fig. 3(a), one can also see that the critical supercurrent has an asymmetry, $I_c^+ \neq I_c^-$, which is referred to as the SRE. Obviously, the asymmetry originates from the combination of the valley coupling effect and the external valley polarization introduced into the system. The physics is not exactly the

same as SRE found in those JJs with both the spin-orbit interaction and external magnetization [47,48]. A salient difference is the fact that a uniform valley coupling cannot even give rise to a ϕ_0 junction, but the spin-orbit interaction does work. This indicates the importance of the interface scattering of the superconductor quasiparticles that results in the possible phase shift or modification to the superconducting phase difference ϕ .

IV. OPTIMAL SRE

As is known, the traveling quasiparticles in the normal G region of the JJ can see the left and right finite *potential barriers*, i.e., the superconducting gap; at least one bound state termed as Andreev bound state (ABS) shall appear and this ABS can carry a supercurrent as

$$I = \sum_{a,b} \frac{\partial E_{a(b)}}{\partial \phi} \tanh(\beta_T E_{a(b)}/2), \quad (8)$$

where E_a and E_b are the ABS energy levels and β_T is the temperature factor. There are generally two sets of ABS since two bands in GS are involved in transport when $\mu > \lambda$ as shown in Fig. 1(b). The simplified ABS in a short junction ($L \ll \xi_s$) has a generic formation as [49]

$$E_{a(b)} = \pm \Delta \sqrt{1 - t_{a(b)} \sin^2(\phi/2 \pm \delta\varphi/2 - \gamma_{a(b)}/2)}. \quad (9)$$

Here, $E_{a(b)}$ is symmetric over $E = 0$ reserving the chiral symmetry, t_a and t_b are the electron transmissions in the normal junction without pair potentials ($0 \leq t_{a(b)} \leq 1$), $\delta\varphi = \delta kL$ denotes the extra shift phase of quasiparticles due to the valley polarization h_z , $\delta k = k^+ - k^- = 2h_z/\hbar v_f$, and moreover, two-type quasiparticles have the opposite phase shifts. Besides, there also exist the phase variations (or phase loss terms) $\gamma_{a(b)}$ when the quasiparticles are reflected in the left GS/S and right G/GS lattice interfaces, which are very subtle to control explicitly unlike the transmission coefficients $t_{a(b)}$. As a matter of fact, the above ABS can be deduced from the quantum condition of the phase accumulation from ϕ , $\delta\varphi$, and γ when quasiparticles traveling in the normal region form a self-closed path [49].

We now present a numerical ABS of the studied JJ in Fig. 4(a), which can be represented by the energy-resolved particle density distribution in the superconductor energy gap $\rho(E) = -\sum_j \text{ImTr}[s_z G_{jj}^r]/\pi$, where the summation of j is limited in the middle G region of the junction. Nevertheless, only a single transverse mode ($k_y = 0$) is plotted in Fig. 4(a). In Fig. 4(b), the simplified ABS from Eq. (9) are plotted for comparison. One can see that the numerical ABS [Fig. 4(a)] can be recovered with suitable parameters $t_{a(b)}$ and $\gamma_{a(b)}$ substituting into Eq. (9).

The two sets of ABSs are separated from each other due to $\delta\varphi$ from h_z , which can account for the appearance of the π -state JJ. The supercurrent reads $I \sim t_a \sin(\phi/2 - \delta\varphi/2) + t_b \sin(\phi/2 + \delta\varphi/2) = t_a \cos(\delta\varphi) \sin(\phi)$ if the transmission coefficients $t_a = t_b$. Oppositely, $t_a \neq t_b$ will lead to the unequal ABS magnitude; as a result, the slopes of two ABS ($\partial E_{a(b)}/\partial \phi$) are unequal, so a ϕ_0 -state JJ is born. Similarly, the phase loss term generally has the same inequality $\gamma_a \neq \gamma_b$, hence they are also contributing to the ϕ_0 phase shift. More

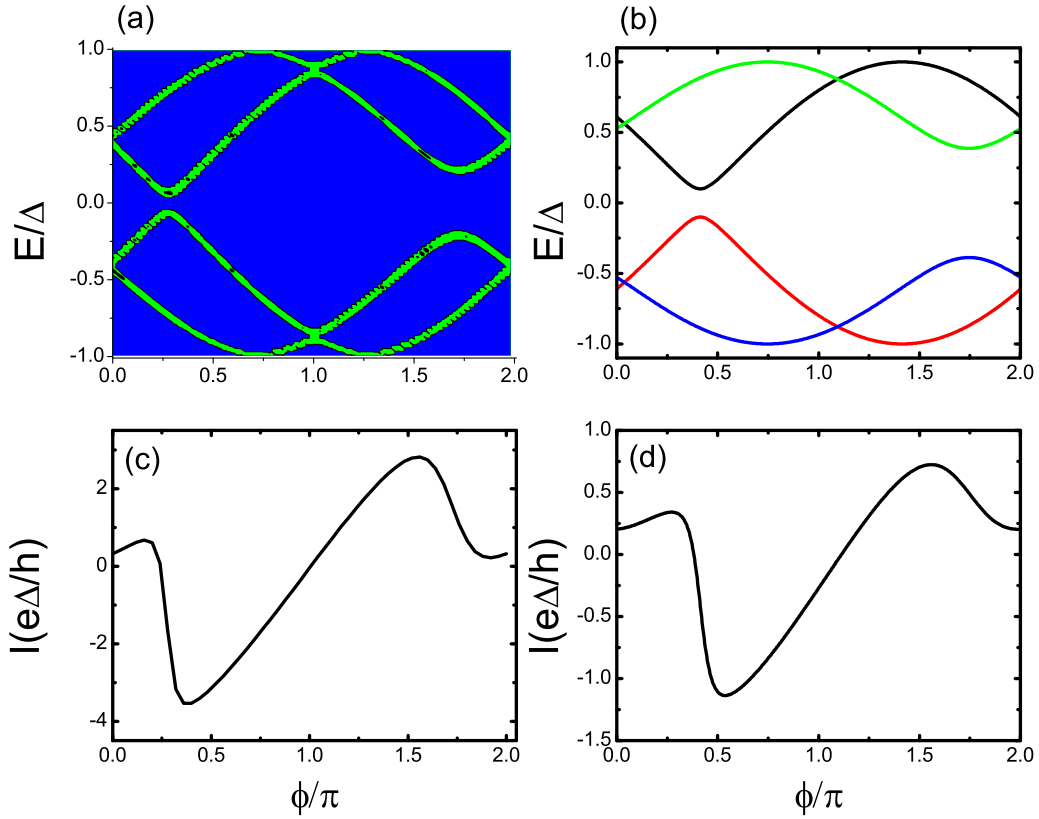


FIG. 4. A single mode ABS from numerical calculations (a) and from the simplified model (b). Numerical parameters in (a) are $k_y = 0$, $\mu = 0.05t$, $\theta = 0.5\pi$, $h_z = 0.02t$, $L = 100a$, and $\lambda = 0.03t$, while the model parameters in (b) are $\gamma_a = 0.2$, $\gamma_b = 0.3$, $\delta\varphi = 0.5\pi$, $t_a = 0.95$, and $t_b = 0.85$. The supercurrents corresponding to the two ABSs are respectively plotted in (c) and (d).

importantly, the critical supercurrent asymmetry ($I_c^+ \neq I_c^-$) is due to this term.

From the simplified ABS in Eq. (9), each ABS by itself can only lead to a symmetric critical current ($I_c^+ = I_c^-$) and no SRE occurs; however, their summation will change the scenario. From Eq. (9), the critical currents I_c^+ and I_c^- for a single ABS case occur around the turning point of the ABS curve but they are equal and no asymmetry. However, the combination of the two ABSs will lead to the inequality $I_c^+ \neq I_c^-$ because the turning point should not be at the same ϕ for both ABS curves due to the phase loss term $\gamma_a \neq \gamma_b$. In Figs. 4(c) and 4(d), the corresponding current phase relations are present for both the numerical ABS [Fig. 4(a)] and the simplified ABS [Fig. 4(b)] cases. As is expected, they resemble each other very much and the SRE is quite conspicuous. Note that the simplified ABS in Eq. (9) neglects the transmission dependence on θ . In fact, when the left and right interfaces of the GS/G/GS junction are asymmetric ($\theta \neq 0$), the transmission of $t_{a(b)}$ would have a weak dependence on θ and thus, even a single ABS can also result in a weak SRE.

According to the simplified ABS model, the SRE would be more evident if the two ABSs had a huge mismatch, i.e., the transmissions for two kinds of quasiparticles have a large difference from each other ($t_a \ll t_b$ or $t_a \gg t_b$). This is similar to the supercurrent interferometers composed of two JJs in Ref. [50] where they have a different interface transparency so that the second supercurrent harmonics [$\sin(2\phi)$] may play

the dominant role and the supercurrent diode can arise. Here, the phase loss term $\gamma_a \neq \gamma_b$ is also vital besides ($t_a \neq t_b$) in the simplified ABS model but it is quite difficult to control efficiently. For the studied JJ, the valley coupling can lead to the band splitting in Fig. 1(b), and the first condition about the transmission can be satisfied: when the universal chemical potential is sweeping just from the lower band to the upper split band, i.e., the JJ would experience the transition from one ABS to two ABSs contributing to the supercurrent, the critical supercurrent asymmetry would exhibit a jump. In other words, when μ just locates around the upper split band bottom as seen in the marked $\pm\lambda$ in Fig. 1(b), the Fermi velocities of electrons in the two bands have a biggest difference, so t_a and t_b would be quite different and the SRE would be maximized. In Fig. 5, we plot the SRE efficiency as a function of the valley coupling strength λ , which is defined as

$$\eta = \frac{|I_c^+ - I_c^-|}{I_c^+ + I_c^-}. \quad (10)$$

It is clearly seen that the SRE has a peak around the chemical potential a little bit larger than λ , $|\mu| \gtrsim \lambda$, i.e., μ is near to the energy bottom of the upper split-band. For $\lambda > |\mu|$, the SRE show a rapid decrease because only one band (a single ABS, spin is neglected) contributes to the supercurrent. However, one can see that even for the latter case, the SRE is still nonzero. In reality, the transmission of electrons in nonsuperconductor junction are weakly dependent on θ ,

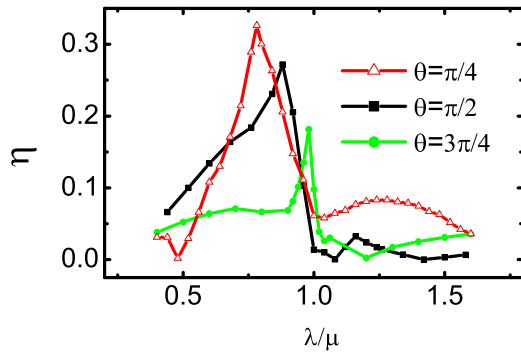


FIG. 5. SRE efficiency η as a function of the valley coupling strength for different θ . Other parameters are $\mu = 0.05t$, $h_z = 0.02t$, and $L = 100a$.

which represents the broken parity symmetry, i.e., the superposition coefficients of two valley-independent states are unequal when the valley-helical eigenstate electrons in the valley-coupled electrodes enter into the middle G region. Such inequality in the studied GS/G/GS junction together with the valley polarization can lead to a weak SRE in the single-ABS case. When the electron energy approaches to the bottom of the uplifted band ($\mu \sim \lambda$) in Fig. 1(b), the difference between t_a and t_b might reach an extremity since the mismatching of

the bands between GS and G is maximum. In addition, the SRE efficiency η shown in Fig. 5 is still low except peaks, and it is also dependent on α or other factors like λ and h_z ; this is mainly ascribed to the blurring effect of many modes contributing to supercurrent since each mode can have different scattering coefficients and phases in Eq. (9).

V. CONCLUSION

In summary, we have investigated the supercurrent rectification effect in the graphene-based JJ by considering the valley-related interactions instead of the spin-related interactions. It is demonstrated that when the nonuniform valley coupling effect from the Kekulé lattice structure is considered in the GS, the introduced valley polarization would lead to a π -state JJ or even a ϕ_0 -state JJ. The forward and backward critical supercurrents are unequal so the SRE can arise. Based on a simplified Andreev bound-state diagram and numerical calculations, we found that the SRE can be maximized as the universal chemical potential locates just above the bottom of the upper split band due to the valley coupling effect.

ACKNOWLEDGMENT

The work is supported by NSFC (Grants No. 12174051 and No. 12174077).

-
- [1] J. M. Raimond, M. Brune, and S. Haroche, *Rev. Mod. Phys.* **73**, 565 (2001); L. Amico, R. Fazio, A. Osterloh, and V. Vedral, *ibid.* **80**, 517 (2008).
- [2] M. A. Nielsen and I. L. Chuang, *Quantum Computation and Quantum Information* (Cambridge University Press, Cambridge, 2000).
- [3] G. B. Lesovik, T. Martin, and G. Blatter, *Eur. Phys. J. B* **24**, 287 (2001).
- [4] N. M. Chtchelkatchev, G. Blatter, G. B. Lesovik, and T. Martin, *Phys. Rev. B* **66**, 161320 (2002).
- [5] J. E. Mooij, T. P. Orlando, L. Levitov, L. Tian, C. H. van der Wal, and S. Lloyd, *Science* **285**, 1036 (1999); Y. Makhlin, G. Schön, and A. Shnirman, *Rev. Mod. Phys.* **73**, 357 (2001).
- [6] A. A. Golubov, M. Y. Kupriyanov, and E. Il'ichev, *Rev. Mod. Phys.* **76**, 411 (2004); A. I. Buzdin, *ibid.* **77**, 935 (2005).
- [7] F. S. Bergeret, A. F. Volkov, and K. B. Efetov, *Rev. Mod. Phys.* **77**, 1321 (2005).
- [8] A. V. Ustinov and V. K. Kaplunenko, *J. Appl. Phys.* **94**, 5405 (2003).
- [9] T. Yamashita, K. Tanikawa, S. Takahashi, and S. Maekawa, *Phys. Rev. Lett.* **95**, 097001 (2005).
- [10] A. K. Feofanov, V. A. Oboznov, V. V. Bol'ginov, J. Lisenfeld, S. Poletto, V. V. Ryazanov, A. N. Rossolenko, M. Khabipov, D. Balashov, A. B. Zorin, P. N. Dmitriev, V. P. Koshelets, and A. V. Ustinov, *Nat. Phys.* **6**, 593 (2010).
- [11] F. Ando, Y. Miyasaka, T. Li, J. Ishizuka, T. Arakawa, Y. Shiota, T. Moriyama, Y. Yanase, and T. Ono, *Nature (London)* **584**, 373 (2020).
- [12] L. Bauriedl, C. Bäuml, L. Fuchs, C. Baumgartner, N. Paulik, J. M. Bauer, K.-Q. Lin, J. M. Lupton, T. Taniguchi, K. Watanabe, C. Strunk, and N. Paradiso, [arXiv:2110.15752](https://arxiv.org/abs/2110.15752).
- [13] J. Shin, S. Son, J. Yun, G. Park, K. Zhang, Y. J. Shin, J.-G. Park, and D. Kim, [arXiv:2111.05627](https://arxiv.org/abs/2111.05627).
- [14] E. Bocquillon, R. S. Deacon, J. Wiedenmann, P. Leubner, T. M. Klapwijk, C. Brüne, K. Ishibashi, H. Buhmann, and L. W. Molenkamp, *Nat. Nanotechnol.* **12**, 137 (2017).
- [15] H. Wu, Y. Wang, P. K. Sivakumar, C. Pasco, S. S. Parkin, Y.-J. Zeng, T. McQueen, and M. N. Ali, *Nature (London)* **604**, 653 (2022).
- [16] C. Baumgartner, L. Fuchs, A. Costa, S. Reinhardt, S. Gronin, G. C. Gardner, T. Lindemann, M. J. Manfra, P. E. Faria Junior, D. Kochan, J. Fabian, N. Paradiso, and C. Strunk, *Nat. Nanotechnol.* **17**, 39 (2022).
- [17] B. Pal, A. Chakraborty, P. K. Sivakumar, M. Davydova, A. K. Gopi, A. K. Pandeya, J. A. Krieger, Y. Zhang, S. Ju, N. Yuan *et al.*, [arXiv:2112.11285](https://arxiv.org/abs/2112.11285).
- [18] M. Davydova, S. Prembabu, and L. Fu, [arXiv:2201.00831](https://arxiv.org/abs/2201.00831).
- [19] N. F. Q. Yuan and L. Fu, *Proc. Natl. Acad. Sci. USA* **119**, e2119548119 (2022).
- [20] A. Daido, Y. Ikeda, and Y. Yanase, *Phys. Rev. Lett.* **128**, 037001 (2022).
- [21] J. J. He, Y. Tanaka, and N. Nagaosa, *New J. Phys.* **24**, 053014 (2022).
- [22] H. D. Scammell, J. I. A. Li, and M. S. Scheurer, *2D Mater.* **9**, 025027 (2022).
- [23] S. Ilić and F. S. Bergeret, *Phys. Rev. Lett.* **128**, 177001 (2022).
- [24] A. A. Reynoso, G. Usaj, C. A. Balseiro, D. Feinberg, and M. Avignon, *Phys. Rev. Lett.* **101**, 107001 (2008).
- [25] H. B. Heersche, P. Jarillo-Herrero, J. B. Oostinga, L. M. K. Vandersypen, and A. F. Morpurgo, *Nature (London)* **446**, 56 (2007).

[26] X. Du, I. Skachko, and E. Y. Andrei, *Phys. Rev. B* **77**, 184507 (2008).

[27] U. C. Coskun, M. Brenner, T. Hymel, V. Vakaryuk, A. Levchenko, and A. Bezryadin, *Phys. Rev. Lett.* **108**, 097003 (2012).

[28] I. V. Borzenets, U. C. Coskun, S. J. Jones, and G. Finkelstein, *Phys. Rev. Lett.* **107**, 137005 (2011).

[29] G. H. Lee, D. Jeong, J. H. Choi, Y. J. Doh, and H. J. Lee, *Phys. Rev. Lett.* **107**, 146605 (2011).

[30] D. S. L. Abergel and T. Chakraborty, *Appl. Phys. Lett.* **95**, 062107 (2009).

[31] T. O. Wehling, A. Huber, A. I. Lichtenstein, and M. I. Katsnelson, *Phys. Rev. B* **91**, 041404(R) (2015).

[32] J. Diez-Merida, A. Diez-Carlon, S. Y. Yang, Y. M. Xie, X. J. Gao, K. Watanabe, T. Taniguchi, X. Lu, K. T. Law, and D. K. Efetov, [arXiv:2110.01067](https://arxiv.org/abs/2110.01067).

[33] Y.-M. Xie, D. K. Efetov, and K. T. Law, [arXiv:2202.05663](https://arxiv.org/abs/2202.05663).

[34] C. Gutiérrez, C.-J. Kim, L. Brown, T. Schiros, D. Nordlund, E. B. Lochocki, K. M. Shen, J. Park, and A. N. Pasupathy, *Nat. Phys.* **12**, 950 (2016).

[35] O. V. Gamayun, V. P. Ostroukh, N. V. Gnezdilov, I. Adagideli, and C. W. J. Beenakker, *New J. Phys.* **20**, 023016 (2018).

[36] C. W. J. Beenakker, N. V. Gnezdilov, E. Dresselhaus, V. P. Ostroukh, Y. Herasymenko, I. Adagideli, and J. Tworzydło, *Phys. Rev. B* **97**, 241403(R) (2018).

[37] J. J. Wang, S. Liu, J. Wang, and J.-F. Liu, *Phys. Rev. B* **98**, 195436 (2018).

[38] J. J. Wang, S. Liu, J. Wang, and J.-F. Liu, *Phys. Rev. B* **101**, 245428 (2020).

[39] M. A. Mojarro, V. G. Ibarra-Sierra, J. C. Sandoval-Santana, R. Carrillo-Bastos, and G. G. Naumis, *Phys. Rev. B* **102**, 165301 (2020).

[40] W. Zeng and R. Shen, *Phys. Rev. B* **104**, 075436 (2021).

[41] G. Giovannetti, M. Capone, J. van den Brink, and C. Ortix, *Phys. Rev. B* **91**, 121417 (2015).

[42] Y. Ren, X. Deng, Z. Qiao, C. Li, J. Jung, C. Zeng, Z. Zhang, and Q. Niu, *Phys. Rev. B* **91**, 245415 (2015).

[43] Q.-P. Wu, Z.-F. Liu, A.-X. Chen, X.-B. Xiao, and Z.-M. Liu, *Sci. Rep.* **6**, 21590 (2016).

[44] F. Zhan, B. Zheng, X. Xiao, J. Fan, X. Wu, and R. Wang, *Phys. Rev. B* **105**, 035131 (2022).

[45] J. Wang, Y. H. Yang, and K. S. Chan, *Phys. Rev. B* **89**, 064501 (2014).

[46] S. Datta, *Superlatt. Microstruct.* **28**, 253 (2000).

[47] A. Rasmussen, J. Danon, H. Suominen, F. Nichele, M. Kjaergaard, and K. Flensberg, *Phys. Rev. B* **93**, 155406 (2016).

[48] J.-F. Liu and K. S. Chan, *Phys. Rev. B* **82**, 125305 (2010).

[49] S. Kashiwaya and Y. Tanaka, *Rep. Prog. Phys.* **63**, 1641 (2000).

[50] R. S. Souto, M. Leijnse, and C. Schrade, [arXiv:2205.04469](https://arxiv.org/abs/2205.04469).